Tuning the Electronic and Magnetic Properties of Nitrogen Functionalized Few Layered Graphene Nanoflakes

Navneet Soin[1,Ψ], Sekhar C. Ray*[,2,Ψ], Sweety Sarma[2], Debarati Mazumder[2], Surbhi Sharma[3], Yu-Fu Wang[4], Way-Faung Pong[4], Susanta Sinha Roy[5], and André M. Strydom[6]

[1]Institute for Materials Research and Innovation (IMRI), School of Engineering, University of Bolton, Deane Road, Bolton BL3 5AB, United Kingdom

[2]Department of Physics, College of Science, Engineering and Technology, University of South Africa, Private Bag X6, Florida, 1710, South Africa

[3]School of Biosciences, University of Birmigham, Edgbaston, B15 2TT, United Kingdom

[4]Department of Physics, Tamkang University, Tamsui 251, Taipei, Taiwan

[5]Department of Physics, School of Natural Sciences, Shiv Nadar University, Gautam Budh Nagar 201314, Uttar Pradesh, India

[6]Highly Correlated Matter Research Group, Physics Department, University of Johannesburg, PO Box 524, Auckland Park 2006, South Africa

[Ψ] These authors contributed equally to this work

Corresponding author:

Prof. Sekhar C. Ray,

Department of Physics, College of Science, Engineering and Technology, University of South Africa, Private Bag X6, Florida, 1710, South Africa

Email: Raysc@unisa.ac.za

ABSTRACT

In this work, we report on the modification of electronic and magnetic properties of few layered graphene (FLG) nanoflakes *via* nitrogen functionalisation carried out using radio frequency (rf-PECVD) and electron cyclotron resonance (ECR) plasma processes. Even though the rf-PECVD N_2 treatment leads to higher N-doping levels in the FLGs (4.06 at%) as compared to the ECR process (2.18 at.%), the ferromagnetic behaviour of ECR FLG(118.62 x 10^{-4} emu/gm) was significantly higher than the rf-PECVD (0.39 x 10^{-4} emu/gm) and pristine graphene (3.47 x 10^{-4} emu/gm). While both plasma processes introduce electron donating N-atoms in the graphene structure, distinct dominant nitrogen bonding configurations (pyridinic, pyrrolic) were observed for each FLG type. While, the ECR plasma introduces more sp^2 type nitrogen moieties, the rf-PECVD process led to the formation of sp^3 coordinated nitrogen functionalities, as confirmed through Raman measurements. The samples further characterised using X-ray absorption near edge spectroscopy (XANES) and X-ray, ultraviolet photoelectron spectroscopies revealed an increased electronic density of states and a significantly higher concentration of pyrrolic groups in the rf-PECVD samples. Due to the formation of reactive edge structures and pyridinic nitrogen moieties, the ECR functionalised FLGs expressed highest saturation magnetisation behaviour with the lowest field hysteretic features. In comparison, the rf-PECVD samples, displayed the lowest saturation magnetisation owing to the disappearance of magnetic edge states and formation of stable non-radical type defects in the pyrrole type structures. Our experimental results thus provide new evidence to control the magnetic and electronic properties of few layered graphene nanoflakes *via* control of the plasma-processing route.

• INTRODUCTION

Intrinsic magnetism observed in materials without *d*- or *f*-electrons has attracted much interest, especially for carbon-based materials and in particular, graphene. There has been a long-standing interest in the development of ferromagnetic graphene for realizing its applications into spintronic devices *via* the combination of spin and charge.[1-4] The introduction of magnetic response in graphene *via* the introduction of edges, vacancy defects or adsorbed atoms has been investigated using both theoretical and experimental means.[1-13] Various theoretical studies.[3-10] have suggested that zigzag edges or point defects in graphene as the spin units should

carry magnetic moment with possible long-range order coupling. This coupling itself can be ferromagnetic or antiferromagnetic, depending on whether the zigzag edges or defects correspond to the same or to different hexagonal sub-lattice of the graphene lattice, respectively. At present, the intrinsic magnetic properties of finite sized graphene sheet are far from being understood, given that the magnetic signal from a finite sized graphene sheet is too weak to be detected by macro-magnetic measurement. Moreover, graphene is intrinsically non-magnetic and lacks localized magnetic moment due to the delocalized π-bonding network, thereby limiting its applications in spintronic devices.[14] Therefore, the induction of magnetic moment and the subsequent synthesis of ferromagnetic graphene or its derivatives with high magnetization are necessary for spintronic applications.

Studies have shown that nitrogen-doping and/or N-functionalization of graphene is an effective route to obtain high magnetization values.[15-21] The nitrogen atom, containing one additional electron, upon replacing the carbon in the graphene lattice[15], can introduce novel electronic properties as well as magnetic moment into graphene.[16] These localized magnetic moments are induced by various arrangements of the N atom, with the pyridine and pyrrole like N-doping defects breaking the degeneracy of the spin polarisation of graphene.[16-19] Indeed, Liu *et al*.[21] have observed high values of magnetization in ferromagnetic graphene oxide (GO), when doped with nitrogen. The substitution by nitrogen of a carbon atom in the graphene lattice leads to an increase in the electronic density of states and the nitrogen dopant can provide π-electron close to the Fermi level of graphene, thereby enhancing the coupling *via* a reduction in the magnetic moment distance.[21,22] Zhang *et al*.[19] proposed that the combination of vacancy defects and N atoms may provide a unique way for enhancing the magnetic moment of graphene. However, experimental evidence from nitrogen-doped graphene for such magnetism remains both scarce and controversial. Moreover, how the different N-bonded species (pyridinic, pyrrolic, graphitic, and adsorbed) affect the electronic and magnetic properties of the host graphene lattice remains controversial. Therefore, the understanding and control of the electronic and magnetic structure of the N-doped graphene is essential for its applications.

In the present study, we have studied the electronic and magnetic properties of few layered graphene (FLG) system functionalized using two different nitrogen plasma processes i.e. electron cyclotron resonance (ECR) and radio frequency plasma enhanced chemical vapour deposition (rf-PECVD). The samples were

characterised using X-ray absorption near edge spectroscopy (XANES), X-ray photoelectron spectroscopy (XPS) and Raman spectroscopy techniques to understand the changes in the electronic and bonding structure. Magnetic property measurements were carried out using a SQUID type magnetometer in conjunction with Magnetic Force Microscopy (MFM), which revealed higher ferromagnetic magnetisation saturation values of the ECR samples (118.62 x 10^{-4} emu/gm), as compared to rf-PECVD samples (0.39 x 10^{-4} emu/gm) and the pristine samples (3.47 x 10^{-4} emu/gm), respectively. Even though the rf-PECVD samples have higher N-doping levels (4.06 at.%) as compared to the ECR samples (2.18 at.%), the ECR plasma leads to the higher concentration of pyridinic nitrogen moieties and stable reactive edge structures leading to pronounced ferromagnetic behaviour.

• EXPERIMENTAL SECTION

Synthesis of FLG: The synthesis of FLG samples was carried out in a SEKI microwave plasma enhanced chemical vapor deposition system, equipped with a 1.5 kW, 2.45 GHz microwave source. The substrates used were bare n-type heavily doped Si wafers (resistivity < 0.005 Ω cm^{-1}) (10 mm x 10 mm). Prior to growth, the substrates were pre-treated with N_2 plasma at 650 W at 40 Torr while the substrate temperature was maintained at 900 ^{o}C. The synthesis was then carried out using CH_4/N_2 (gas flow ratio = 1:4) plasma at 800 W for a duration of 60 s. The FLG samples were then allowed to cool down to ambient temperature under a constant N_2 flow. The synthesis conditions used here are similar to the ones reported in our earlier works.[28,33]

Nitrogen plasma doping of FLGs: Nitrogen doping/functionalization of FLG was carried out using two separate procedures: rf-PECVD and ECR. The ECR treatment offers the advantages of high dissociation percentage of process gas (N_2) and high uniformity of plasma energy over large areas. During the ECR treatment, the chamber was pumped down to a base pressure better than 7 x 10^{-5} Torr using a combination of a turbo molecular and rotary pump. The condition at which resonance occurs for electrons is a function of the excitation frequency of the alternating electric field and the strength of the static magnetic field. In our system, as mentioned before, the excitation source is 2.45 GHz and the strength of the static magnetic field is 875 G. For sufficient resonance to occur, the process pressure should be sufficiently low. For N doping, we have used a working pressure of ~0.025 Pa (1.8 x 10^{-4} Torr) and the microwave power was maintained at 150 W (samples

named as FLG:N(ECR) for a duration of 5 min [28]. Similarly, for an another set of samples, the post-deposition N-doping process was carried out in a rf-PECVD chamber (samples named as FLG:N(PECVD)) using N_2 at low pressure ~ $2x10^{-6}$ Torr at a power of 200 W.[34]

Characterisation: Raman spectroscopy was performed using an ISA LabRam system equipped with a 632.8 nm He-Ne laser with a spot size of approximately 2-3 µm, yielding a spectral resolution of better than 2 cm^{-1}. Due care was given to minimize sample heating by using a low laser power below 2 mW. The XPS spectrum was measured on a Kratos Axis Supra DLD employing an Al Kα radiation (1486.6 eV). The XANES spectra was obtained using the high-energy spherical grating monochromator 20A-beamline at the National Synchrotron Radiation Research Centre (NSRRC), Hsinchu, Taiwan. The magnetic properties of these FLGs were characterized by a SQUID type magnetometer with sensitivity better than $5x10^{-8}$ emu. The topographical and magnetic force microscopy (MFM) measurements were carried out using a Veeco Dimension 3100 AFM connected to a Nanoscope IIIa controller in the tapping mode configuration. To detect magnetic domains in the prepared samples, low moment magnetic probes with Co/Cr coatings were used. In addition, the electron field emission (EFE) was measured using a Keithley source meter.

• RESULTS AND DISCUSSION

Fig. 1(a) shows the Raman spectra of pristine and rf-PECVD, ECR treated nitrogen-functionalized FLGs within the 1200–3000 cm^{-1} range. For carbon materials, the main Raman spectral features are the D (~1350 cm^{-1}) and G (1580 cm^{-1}) bands, respectively. While, the G band corresponds to the optical E_{2g} phonons at the Brillouin zone center; the D peak arises due to the breathing-like modes (corresponding to TO phonons close to the K point) and requires a defect for its activation *via* an inter-valley double resonance Raman process. The intensity of the D-band provides a simple measure of the amount of disorder in graphene and graphene based structures. The overtone, 2D band, appears at around 2670 cm^{-1}, being the sum of two phonons with opposite momentums and acts as the fingerprint for monolayer graphene and is present even in the absence of any defects.[23-27] The D′ peak observed at ~1620 cm^{-1}, occurs *via* an intra-valley double resonance process in the presence of defects. Since the D band requires a defect to be Raman active, it is generally not used to characterize the heteroatom doping. However, both the G and 2D bands are both strongly influenced by the

carrier concentration and have been extensively used for doping characterization.[23-27] Detailed analysis of peak positions and the full width at half-maximum (FWHM) parameters was carried out by fitting the first and second order Raman spectra using Lorentzian (for D, G, and G` bands), and Gaussian (for D`) peak shapes.[28,33] Now, as compared to the peak position (~1582.2 cm^{-1}) and the FWHM (35.6 cm^{-1}) of the G band in pristine FLGs; upon nitrogen doping, the G band upshifted slightly to 1581.5 cm^{-1} (for FLG:N(PECVD) samples) and 1581.7 cm^{-1} (for FLG:N(ECR) samples) with a corresponding increase in the D band position from 1329.9 cm^{-1} (pristine FLG) to 1335.3 cm^{-1}, respectively. It should be noted that although the G band peak shifts are more prominent in electrostatically gated mono-layered graphene, nevertheless, similar stiffening of the G band along with FWHM enhancement has been previously observed in chemically doped graphene as well.[28-30] This blue shift of the G band (E_{2g} mode at Γ) along with the associated broadening of FWHM has been attributed to the non-adiabatic removal of the Kohn anomaly from the Brillouin zone centre, G.[28-30] The ECR plasma treatment induces the substitution of electron-donating nitrogen atoms into the graphene lattice, with the overall effect of a rise in the Fermi level that is then observed in the blue shift of the G band in Raman spectra.[28] The incorporation of N into the FLG structure may generate C–N and N–N bonds at the expense of the C–C bonds. However, the C–N vibration modes, which lie between the D and G bands, cannot be identified owing to the insensitivity of the Raman excitation to distinguish between the cross sections of C and N atoms. For electric field gated graphene, by applying suitable bias, both electron and hole conduction mechanisms are accessible, by shifting the Fermi level and can be observed in the upshift of the G peak in the Raman spectra for both the cases.[30] Similarly, the 2D band shows an upshift from 2660.4 cm^{-1} (pristine FLG) to 2661.2 cm^{-1} (for FLG:N(ECR) and further to a value of 2663.8 cm^{-1} (for FLG:N(PECVD)), with a slight increase in the FWHM from 43.7 cm^{-1} to 44.0 cm^{-1} (44.3 cm^{-1}). This is accompanied by the change in the I_D/I_G (I_{2D}/I_G) ratio to 1.03 (0.80) from 0.83 (1.02) for pristine FLGs and as mentioned earlier signifies the formation of FLGs. This blue shift of the 2D band has also been observed by Yan *et al.*, and has been attributed to the increased disorder and reduction in the crystallinity in N-doped graphene and is consistent with those observed in electrostatically gated graphene.[30,31]

In a recent work by Eckmann *et al.*, the I_D/I_D' ratio of graphene was used to comment on the nature of induced defects through fluorination and Ar^+ bombardment.[32] In their study, it was observed that the I_D/I_D' ratio was

maximum (~13) for sp^3 type defects and reaches a minimum (~3.5) for boundaries in graphite.[32] In our study, the I_D/I_D' ratio varied from 3.03 for pristine FLGs vs. 3.44 for FLG:N (ECR) and further increased to 4.19 for FLG:N(PECVD) samples. The rather high value of I_D/I_D' for the pristine samples can be attributed to the finite crystallite size and the presence of boundaries, the combination of which leads to the defect induced D peak as well. While both the N-treated FLGs were prepared using plasma modification, the difference in the working conditions as well as the power leads to significant differences in the formation of defects. The electron-cyclotron resonance conditions used for functionalisation produces N^+ bombardment, which produces substitutional and vacancy-like defects in the graphene lattice. However, the number of defects produced in the graphene lattice are limited due to the lower ion energy of the species.[28] It can be observed that the rf-PECVD nitrogen process introduces more sp^3 type defect structures into the graphene lattice unlike the ECR process. A similar reduction in the structural order has been previously by Abbas et al in their study of the rf-PECVD N_2 functionalised vertically aligned carbon nanotubes.[34] It should be mentioned that since the FLG are vertically aligned on a Si-substrate, it is expected that only the top-most surfaces of the FLG would be predominantly accessible to atomic nitrogen during the functionalization procedure.

Fig. 1(b) shows the plot of EFE current density (J) as a function of the applied electric field (E_A) for pristine FLG and FLG:N samples. The figure shows the existence of a classical threshold electric field at which the current density, J, increases significantly from a zero value. As compared to pristine FLGs, the threshold electric field is reduced for FLG:N(ECR) samples; whereas for FLG:N(PECVD) samples, the threshold value increases; suggestive of the fact that for FLG:N (PECVD) samples the required activation energy is enhanced whereas the ECR N-treatment reduces the required activation energy for the tunnelling of electrons. The Fowler–Nordheim (F–N) plots shown in Fig. 1(f) clearly show the existence of turn-on electric field (E_{TOE}) which was measured by linear fitting of the curve in the high electric field region. For pristine FLGs, the E_{TOE} value was 26.5 V μm^{-1}; which further increased (decreased) to 40.0 (20.0) V μm^{-1} for PECVD (ECR) N-treated graphene samples, respectively, owing to the increase (decrease) in the sp^3-hybridized bonds in graphene structures.[33,35,36] It must be noted that the N-doping levels in the FLG:N (ECR) samples (~2.18 at%) are only half of that in the FLG:N (PECVD) sample (~4.06 at%). It is expected that with an increase in the nitrogen content of the carbon nanostructures, the electron field emission should increase concurrently. The sp^2

hybridised bonds, upwards movement of the Fermi level (discussed later) as well as the creation of defect sites in the FLG:N(ECR) samples are responsible for the enhancement of electron field emission current; whereas for the FLG:N(PECVD) samples, comparatively higher sp^3 bonding configuration is observed in the Raman analysis.[28,33,37] Thus, the reduction of the EFE current in rf-PECVD N-treated graphene is due to the decrease of the number of sp^2 hybridized bonds in the network which is responsible for the metallic EFE current.[38,39] These results further substantiate that the rf-PECVD plasma treatment promotes the three dimensional sp^3 bonding configuration; whereas the ECR N-doping promotes the more desirable sp^2 bonding configuration[34,37,38] and further establishes that for field emission, the nitrogen bonding configuration in doped graphene is the dictating factor rather than the absolute nitrogen content.

For graphitic materials in general, the XANES spectra can be divided into three regions as characterized by their specific resonance energies.[40] The first region of π* resonance appears around 285±1 eV, the C–H* resonance around 288±1 eV, and finally a broad region corresponding to the σ* resonance appears between 290 and 315 eV. The presence of the π* and C–H* resonances serve as a fingerprint for the existence of sp^2 hybridized C–C bonds and C–H bonds, respectively. Fig. 2 shows the C *K*-edge XANES spectra of the pristine and N-functionalised FLGs with spectral features at ~285.1 (±1) eV, ~291.6 (±1) eV and ~292.6 (±1) eV; attributed to the unoccupied 1s→π*, excitonic states and 1s→σ* transitions, respectively.[40,41] As observed from the first order derivative (top inset Fig. 2a) of the C *K*-edge spectra, the absorption edges of the nitrogen functionalized graphene are shifted towards higher (lower) energy levels for the rf-PECVD (ECR) N-graphene samples indicating the presence of less (more) sp^2-rich structures. This change in the absorption edge is attributed to the change in the band gap of the N-FLG samples due to the structural rearrangement *via* the bonding of nitrogen with the host carbon lattice.[41,42] Apart from the π* and σ* resonance peaks, two other peaks observed at ~288.0 eV and ~289.3 eV are ascribed to C–H bonds and interlayer graphite states, respectively (shown as inset below in Fig. 2a). As compared to the pristine FLG and FLG:N(PECVD) spectra, the FLG:N(ECR) sample shows an enhanced feature at ~288 eV, accompanied by a prominent peak in the interlayer graphite peak intensity. While, Ray *et al.* have observed a similar feature in the 287-291 eV range for amorphous a-C:H(OH) thin films and attributed it to a combination of the C-H σ* bonding with the O-

C=C, C-OH and C=O π* bonds.[35,41] Pacile *et al.* have attributed it to the splitting of the π* bands in graphene and to interlayer state related to the charge density between graphene layers.[43] Nevertheless, for the FLG:N(PECVD) samples, the increase in the feature at ~288 eV can be attributed to the increase in the C–H intensity which indicates the formation of sp^3-rich structures having a higher content of C–H bonds, thus confirming the Raman and EFE analysis of the previous section. In the case of FLG:N(ECR) samples, the C *K*-edge XANES spectrum shows a strong peak at 0.2 eV below the interlayer graphite peak (marked with a line bar), which may arise from the contribution of N- and O-related bonds in N-graphene. For the rf-PECVD N-functionalized samples, the C *K*-edge XANES spectra show that both the π* and σ* peaks are wider and show an upward energy shift which is different from ECR N-graphene again indicating a change in the band gap of the material.

It is well established that the introduction of nitrogen into the sp^2 graphene lattice leads to the appearance of various nitrogen moieties. For N-doping in graphene and carbon nanotubes largely three type of bonding has been observed: (i) direct substitution (graphitic N), (ii) pyridinic and (iii) pyrrolic configuration.[44] In the graphitic configuration, three nitrogen valence electrons form three σ-bonds, one electron fills the π–state while the fifth electron enters the π∗ state of the conduction band, leading to strong n-type doping effect. Similarly, for CNTs, DFT calculations have shown an increase in the Fermi level for graphitic N doping, thereby increasing the metallicity; whereas, upon pyridinic and adatom configurations (p-doping) in CNTs, a reduction in the Fermi level has been reported.[44] Similarly, for pyridinic and pyrrolic type N-doping in graphene, the situation becomes complicated. For example, the simple tight-binding models do not predict any charge transfer effects whereas in some studies, the p-type doping induced by these groups have shown some charge transfer, however its magnitude is much smaller than that for graphitic nitrogen.[44] Fig. 2(b, c) shows the N *K*-edge XANES spectra of the FLG:N samples wherein the intensity of the main π* peak reflects the N-doping content i.e. lower peak height for FLG:N (ECR) as compared to FLG:N(PECVD). This can be described *via* the delocalisation of the π* states with N $2p_z$ orbital components providing much smaller transition dipole moment values between the N1s orbitals.[45] The π* region of N *K*-edge XANES spectrum was deconvoluted into four components using Gaussian line shapes, as shown in Fig. 2(c, d) reflecting the

spectral evidence for the local electronic states bound to the nitrogen site. For the FLG:N(ECR) samples, the N *K*-edge XANES spectrum shows four peaks located at ~396.6, ~397.7, ~398.7 and ~399.9 eV. These peaks can be attributed to nitrogen in nitride phase, pyridine-like bonding and pyrrole/substitutional graphite like bonding, respectively.[46] Pyridinic-N refers to nitrogen atoms at the edge of graphene planes, each of which is bonded to two atoms and donates one π-electron to the aromatic π system, while quaternary nitrogen is also called graphitic nitrogen or substituted nitrogen, in which nitrogen atoms are incorporated into graphene layer and replace carbon atoms within the graphene sheet. Geng et al. have observed similar peak positions in their study of nitrogen doping effects on the structure of graphene.[46] The π* resonance peak at 397.7 eV, attributed to pyridine-like bonding, arises due to transitions from the *K*-shell (N 1s) to the unoccupied π* orbital.[48,49] The peak position of the pyridine like species is however 1.0 eV lower to that reported by Liu *et al*. in the case of nitrogen doped graphene oxide[21,47] and that by Usachov *et al*. in their study of N-graphene synthesised from s-triazine molecules.[44]

Comparing the deconvoluted N *K*-edge spectra of the N-functionalised samples (Figs 2(c, d)), the most significant difference observed is the peak III (attributed to pyrrolic nitrogen), thus indicating higher pyrrole-like bonding for FLG:N (PECVD) samples. It has also been reported that the pyrrolic N atoms bonds with the sp^3 C atoms, forming five-membered heterocylic rings which lead to a reduction in the Raman 2D band intensity.[50] This correlates well with the observed reduction in the Raman 2D band for the FLG:N(PECVD) samples (Fig. 1(a) and Table 1), thus further confirming the enhanced formation of pyrrolic bonding for FLG:N(PECVD) samples.[50] In their study, Zhao *et al.*[51] have utilised low-energy nitrogen bombardment (25-150 eV) followed by high temperature annealing (~ 900 K) to produce nitrogen doped graphene. It was revealed from their work, that a variation of the ion-beam energy not only resulted in the variation of nitrogen doping content but also in the preferential bonding, wherein, at increased ion energies and time, a relative increase in the pyridinic nitrogen was observed. Sakulsermsuk *et al*. too have reported that at higher ion energy, nitrogen ions prefer forming pyridinic-N rather than pyrrolic-N groups.[52] It must be emphasised that during the course of this work, the ion energy during the plasma bombardment was not measured; however previous work has established that the ECR systems typically generate high density plasma at much lower potentials due to the resonance heating of the electrons. In fact, the magnetic field induced electron

confinement in the ECR configuration generates high temperature electron distribution tails of nearly 30 eV which lead to a relatively high degree of N_2 dissociation without a significant increase in the potential or ion bombardment energies.[53] Considering that for both set of samples, the treatment time was kept the same; the ECR process produced significantly higher pyridinic nitrogen as compared to the rf-PECVD process and as such corroborates the results presented by Zhao *et al.*[51] Using molecular dynamics, Åhlgren *et al.* have reported on the possible events occurring during the plasma functionalisation of graphene, including the formation of vacancy defects and substitution of carbon by nitrogen.[54] It is understood that the most stable N-dopant configuration in graphene is associated with the strain generated from structural defects as well as vacancy defects.[52,54] The structural vacancies themselves are introduced into the graphene structure during the growth process as well as under the plasma functionalisation process. In the case of edge defect, dominated FLG samples (Fig. 1(a), Table 1), the most typical defects which appear upon plasma functionalisation include the mono and di-vacancy. From the calculations carried out Ahlgren *et al.*, it was observed that lower ion energies tend to produce mono-vacancies whereas higher ion energy induces di-vacancies.[54] Moreover, DFT simulations show that pyridinic-N provides the most stable N-dopant configuration for mono-vacancy defects, whereas, for di-vacancy, it is pyrrolic-N configuration which is the most stable.[52,54] Thus, for FLG:N(PECVD) and FLG:N(ECR) samples, a higher pyrrolic and pyridinic content are expected and indeed observed. However, further experimental studies are required to study the effect of the ion energy on the stable nitrogen configuration in FLGs.

Figures 3(a-h) shows the C, O and N 1*s* core-level XPS spectra for the individual chemical binding environment in pristine and nitrogen functionalized FLG samples. In Fig. 2(a), the wide-width asymmetric C 1*s* complex band of FLG shows three deconvoluted peaks *viz.* 284.5 (C1), 285.4 (C2) and 287.4 eV (C3), respectively corresponding to C=C, C-OH/C-H and C=O, respectively. Fig. 2(b, c) shows the three convoluted characteristics peaks *viz.* 284.6 (C1), 285.0 (C2), 286.9 (286.4) (C3) and are assigned as C=C, C=N and C≡N respectively for the FLG:N (PECVD/ECR) samples, respectively.[55] It is also observed that the C=C peak is reduced for FLG:N samples, confirming the formation of C=N and C≡N bonding after nitrogen functionalization. The oxygen-functionalized groups are gradually reduced from the FLG to N-FLG structure with N-doping. This change of oxygen functional groups is observed from the O 1*s* XPS spectra as shown in

Fig. 3(d-f). Figure 2(d-f) shows wide asymmetric O 1*s* core-level XPS spectrum complex band composed of different oxygen-related bonds for FLG transform into less intense features in N-FLG. After well-convoluted into two peaks, we have C-OH at ~532.4 (±0.1) eV and C-OOH at ~533.2 (±0.2) eV, which are at the edge of aromatic structure.[56] In Fig. 3(g,h), the intensity of N 1*s* XPS spectrum is increased at higher nitrogen concentration. The N 1*s* spectra of ECR (PECVD) N-FLGs are deconvoluted into three (four)-peaks and are centred at peak I: ~398.3 (397.9) eV, peak II, ~399.7 (399.4) eV, Peak III 401.1 (400.5) eV; which are assigned to the pyridinic N at the edge of six-member ring, pyrrolic N structure at the edge of five-member ring and quaternary N structure, respectively.[57] In addition, peak IV at ~ 402.0 eV is observed in N 1*s* spectra of N-FLGs functionalized in PECVD process and is assigned as graphitic-N. It is observed that the pyrrolic-N content is higher in rf-PECVD samples than ECR- nitrogen functionalized FLG samples.[57] However, it is also observed from the above results that the intensity of oxygen-related functional groups in C 1*s*/O 1*s* XPS spectra are decreased; whereas the intensity of N 1*s* XPS spectra is increased with increase of nitrogen content in the N-FLG. These results suggest clearly that the removal of oxygen functional groups (C=O and C-OH) and increase of nitrogen-related pyrrolic, pyridinic, quaternary-N and graphitic-N groups in the N-FLG samples.

Ultraviolent photoemission spectroscopy (UPS) scans of pristine and nitrogen functionalized FLGs along with Ag (as reference) are shown in Figure 4(a); wherein the Fermi edge is clearly visible. The valence band maximum (VBM) of pristine FLG and nitrogen functionalized FLGs are estimated from the extrapolation at the edge of UPS (He-I) spectra. It was observed that the VBM of pristine FLG is 4.2 eV, while for the FLG:N samples functionalized by ECR and rf-PECVD processes, the VBM values are 4.0 and 3.8 eV, respectively. This reduction in the VBM upon nitrogenation occurs owing to the n-type doping and formation of N-lone-pair electron, π-electrons of C-N bonds, σ-electrons of C-N bonds and the consequential structural rearrangement inside the pristine FLG structure.[58] To further study the electronic density of states (DOS) of these samples; we have studied the total DOS below the Fermi level (E_f) by using UPS (He-II). As shown in Fig. 4(b), both the FLG:N samples shows higher DOS than the pristine FLGs. Figure 4(c-e) shows the deconvolution of UPS He-II spectre into five distinct hybridized bands: C 2*p*-π at ~4.3 eV (I), C 2*p* σ+π at 6.0 eV (II), C 2*p*-σ at 8.4 eV (III), C 2*s*-2p at 10.8 eV (IV) and C 2s- σ at 13.9 eV (V) for both pristine and

nitrogen functionalized FLG.[59] The features at 8.4, and 6.0 eV are considered as the π bonding of C=O and O lone pair [60] that overlaps with C 2*p*-(σ+π) and C 2*p*-σ aromatic features of FLG.[57] It is observed that after the nitrogen plasma treatment, while the peak I is reduced for both rf-PECVD and ECR processes, the peak II is reduced (enhanced) for the PECVD (ECR) process. This peak II at ~7.0 (6.4) eV can be attributed to the combination of nitrogen-bands, C=N and N lone pair for FLG:N.[61,62]

The magnetic properties of the FLG and FLG:N samples were measured in the range of -2kOe<H<2kOe at temperatures of 300 K and 40 K, respectively. The measured magnetic hysteresis loops are shown in Fig. 5, with the FLG:N (ECR) samples (Fig. 5(c)) showing the most expressed ferromagnetic behaviour with lowest field hysteretic features (H_c = 40 Oe) and highest saturation magnetisation (M_s = 118.62 x 10^{-4} emu g^{-1}); whereas the rf-PECVD samples shows the lowest saturation magnetisation (M_s = 0.39 x 10^{-4} emu g^{-1} and H_c = 80.3 Oe). As compared to the pristine FLGs (M_s = 3.47 x 10^{-4} emu g^{-1}), the magnetic moment values of FLG:N(ECR) (Fig. 5(c)) are the highest owing to the incorporation of nitrogen in the graphitic structure of FLG as observed in C *K*-edge and N *K*-edge XANES spectrum. This enhanced magnetism is due to the extra π-electron from nitrogen making the structure electron-rich, thereby, enhancing the magnetic coupling between magnetic moments.[21] In their recent work, Miao *et al*. observed enhanced ferromagnetism in N-doped graphene with an increase in the saturation magnetisation and coercive field with an increase in the nitrogen content, especially pyrrolic groups of the samples which can induce a net magnetic moment of 0.95 μ_B/N.[63] In contrast, Ito *et al*. have observed that the presence of pyrrolic groups lead to a reduction in the magnetisation values.[64] Previously, He *et al*., reported that the magnetisation of the $^{12}C^+$ implanted highly oriented pyrolytic graphite was found to be closely correlated with the density of defects and an almost linear relationship between the I_D/I_G ratio and saturation magnetisation was observed.[65] As the FLG:N(ECR) graphene shows the highest I_D/I_G ratio, it is expected and indeed observed that the N-graphene displays highest magnetization values. For N-graphene, the Fermi level shifts upwards due to the extra π electron making graphene electron-rich.[66] The shift of C *K*-edge and formation of different carbon–nitrogen bonds observed in the N *K*-edge XANES spectra clearly indicated the formation of *p* electron and Fermi level shift. The high value of I_D/I_G ratio of N-graphene also implies defect rich N-graphene. The result suggests that the magnetic properties of these structures are entirely determined by the graphitic region due to the π character of the spin density. Thus,

N-doping enhances the direct type of magnetic coupling between the magnetic moments due to the decrease in the distance between the magnetic moments. Moreover, the presence of magnetic exchange or coupling between the localized magnetic moments is a necessary ingredient for the magnetic cooperative behaviour such as ferromagnetic ordering. It is noted that the specific contribution made by each specific type of two N types (pyridinelike and cyanide-like) is complicated, and it is difficult to clarify the specific contribution in N-graphene.

It is expected that at higher nitrogen concentrations, the defect formation along with the incorporation of nitrogen atoms in the graphitic phases can give rise to the presence of lone pair electron spin leading to the possibility of ferromagnetic ordering and increased saturation magnetisation.[67] Why the FLG:N(PECVD) samples with higher nitrogen content (see table 1) show anomalously lower magnetisation than even the pristine FLG is still not entirely clear as yet. As discussed above, in their recent report Ito *et al*.[64], observed that upon pyrolysis of nitrogen containing pre-halogenated carbon precursor, a reduction in the magnetic properties of graphene domains occurred. In their study, the decrease in the magnetism was attributed to multiple factors, including appearance of diamagnetic features and disappearance of magnetic edge states i.e. radical-type edge states in six-membered heteroatom ring structure occurring due to the additional electron density supplied by nitrogen atoms on pyridinic and graphitic positions. Furthermore, invoking the stability influence of various bonding states, it incorporation of nitrogen into a 5-membered ring structure i.e. pyrrole type structure, led to a stable non-radical type defects reducing the overall magnetism via a reduction in the ferromagnetically active defect density. In their work on ferromagnetism in nitrogen doped graphene, Błoński et al too have considered the effects of pyrrolic nitrogen in introducing magnetism in graphene.[68] In their DFT studies, it was observed that introduction of pyrrolic nitrogen into the graphene lattice had no effect and the subsequent coupling between pyridinic nitrogen moieties did not result in any long-range magnetic ordering. In the present study, for the FLG:N(PECVD) samples, it was indeed observed that the amount of pyrrolic nitrogen was significantly higher than the FLG:N(ECR) sample which may contribute to the reduction of magnetism to even lower levels than that of the pristine FLGs.[61]

Further detection of the magnetic domains in the pristine and FLG:N(ECR) samples was carried out using magnetic force microscopy (MFM) measurements employing low magnetic moment probes with Co/Cr

coating. The magnetized Co/Cr coated probe interacts with magnetic field gradients generated by magnetic domains within the synthesised FLGs resulting in observable changes in the phase and amplitude of the oscillating cantilever. Fig. 5 (d-f)/(g-i) and Fig. 5 (j-l)/(m-o) show the topographic (height), amplitude and phase signals imaged simultaneously for both tapping mode AFM and magnetic force microscopy (MFM) mode to assess the correlation of surface features, identify and eliminate possible artifacts and to assess the effects of nitrogenation on magnetization. To assess the correlation of surface features and the effects of magnetization, the topographic (height), amplitude and phase signals were imaged simultaneously for both conventional topographical imaging and magnetic measurements. MFM data were acquired while maintaining a constant "lift scan height" of ~10 nm above the topography (height) data to reduce the coupling between van der Waals and magnetic forces and to demonstrate the field strength generated by the magnetic domains. In the "lift-scan" mode, the topography is measured in the dynamic amplitude modulation mode after which the tip is then moved at a constant distance above the surface during which the magnetic component of the data is recorded.[33] In theory, the topographic contributions should get eliminated in the second image. Comparing the AFM scans of the samples with the MFM scans, while no significant changes are observed in the topographic signal; significant differences are observed in the phase and amplitude scans. For the conventional AFM scans, the phase signal is essentially a map of how the phase of the cantilever oscillation is affected by its interaction with the sample surface and is affected highly by topography among other factors such as chemical nature, relative hardness/softness of the sample. Since the MFM signal represents the phase shift between the probe oscillation and the driving signal due to magnetic force acting on the tip, therefore by visualising/measuring the changes occurring in the amplitude and phase images, the existence of magnetic domains in the samples can be ascertained. For a true quantitative interpretation of the MFM images, it is necessary to have precise knowledge of the geometry, magnetic properties of the tip and the tip-sample interactions to express the force acting on the tip, which has only been achieved in special cases.[10] Nevertheless, a qualitative analysis can be carried out by considering the phase and amplitude changes observed in the MFM images as shown in Figure 5(j-l)/(m-o). It should be noted that an attractive interaction between the between the tip and the sample leads to a negative phase shift (dark contrast), while a repulsive interaction will lead to a positive phase shift (bright contrast). In fact, the MFM phase and amplitude images

show a very good correlation in the formation of the magnetic domains. For all the FLG samples, the magnetic domains appear as dark and bright-localized regions in the phase and amplitude images respectively. Considering Figure 5(j-l)/(m-o), representing amplitude images of pristine FLG and ECR N-graphene, it can be clearly observed that the magnetic domains in the ECR N-graphene are more localized than in the case of pristine FLG. A simple visual scaling of MFM phase data suggests that the ECR N-graphene the strongest magnetization effect, which is consistent with the M–H magnetization results discussed above.

• CONCLUSIONS

In summary, we have observed room-temperature ferromagnetism for both pristine and nitrogen plasma functionalised FLGs. The dependence of the magnetic properties on the electronic and chemical bonding nature of nitrogenated species was elucidated using X-ray based spectroscopic techniques. The XANES measurements suggest that the magnetic properties of the FLGs are entirely determined by the graphitic region due to the π character of the spin density wherein the N-doping enhances the direct type of magnetic coupling between the magnetic moments due to the decrease in the distance between the magnetic moments. More specifically, considering the various bonding states, the incorporation of nitrogen into pyrrolic structure leads to the formation of stable non-radical type defects, which, as compared to the pristine FLGs, reduced the magnetism for rf-PECVD nitrogen functionalised samples. For the ECR nitrogen functionalised samples, the enhanced magnetism is due to the extra π-electron from nitrogen making the structure electron-rich, thereby, enhancing the magnetic coupling between magnetic moments alongside the increased defect density as measured from Raman spectroscopy. The intrinsic room-temperature ferromagnetic character of the materials, but without the constraint of spontaneous magnetization, combined with its semi-conductivity and functionalization capability, should have wide-reaching implications in material science, and these collective properties could make graphene-based materials a competent choice for many important device applications, including spintronics, magneto-resistance, and magnetic memory devices, among others.

• ASSOCIATED CONTENT

Supporting Information: The Supporting Information is available free of charge on the ACS Publications

• AUTHOR INFORMATION

Corresponding author

* E-mail: Raysc@unisa.ac.za

Notes

The authors declare no competing financial interest.

• ACKNOWLEDGEMENTS

The author S.C.R. and S.S. acknowledges to National Research Foundation, South Africa (Grant No. EQP13091742446 and PD-TWAS150813137166) for financial support. AMS thanks the SA-NRF (93549), the FRC and URC of UJ for financial assistance. D. Britz is thanked for his assistance with the magnetic measurements.

• REFERENCES

(1) Yazyev, O. V. Emergence of magnetism in graphene materials and nanostructures. *Rep. Prog. Phys.*, **2010**, *73*, 056501:1-16.

(2) Nair, R. R.; Sepioni, M.; Tsai, I.-L.; Lehtinen, O.; Keinonen, J.; Krasheninnikov, A. V.; Thomson, T.; Geim, A. K.; Grigorieva, I. V. Spin-half paramagnetism in graphene induced by point defects. *Nat. Phys.*, **2012**, *8*, 199–202.

(3) Yazyev, O. V.; Katsnelson, M. I. Magnetic Correlations at Graphene Edges: Basis for Novel Spintronics Devices. *Phys Rev Lett*, **2008**, *100*, 047209:1-4.

(4) Soriano, D.; Munoz-Rojas, F.; Fernandez-Rossier, J; Palacios, J. J. Hydrogenated graphene nanoribbons for spintronics. *J. Phys Rev B*, **2010**, *81*, 165409:1-7.

(5) Joly, V. L. J.; Takahara, K.; Takai, K.; Sugihara, K.; Enoki, T.; Koshino, M.; Tanaka, H. Effect of electron localization on the edge-state spins in a disordered network of nanographene sheets. *Phys. Rev. B*, **2010**, *81(11)*, 115408:1-6.

(6) Yazyev, O. V.; Helm, L. Defect-induced magnetism in graphene. *Phys Rev B*, **2007**, *75*, 125408:1-5.

(7) Jung, J.; Pereg-Barnea, T.; MacDonald, A. H. Theory of Interedge Superexchange in Zigzag Edge Magnetism. *Phys Rev Lett*, **2009**, *102*, 227205:1-4.

(8) Fujita, M.; Wakabayashi, K.; Nakada, K.; Kusakabe, K. Peculiar Localized State at Zigzag Graphite Edge. *J Phys Soc Jpn*, **1996**, *65*, 1920-1923.

(9) Ma, Y. C.; Lehtinen, P.O.; Foster, A. S.; Nieminen, R. M. Magnetic properties of vacancies in graphene and single-walled carbon nanotubes. *New J. Phys*., **2004**, *6*, 68:1-15

(10) Cervenka, J.; Katsnelson, M. I.; Flipse, C. F. J. Room-temperature ferromagnetism in graphite driven by two-dimensional networks of point defects. *Nat Phys*, **2009**, *5*, 840–844.

(11) Wang, Y.; Huang, Y.; Song, Y.; Zhang, X.; Ma, Y.; Liang, J.; Chen, Y. Room-Temperature Ferromagnetism of Graphene. *Nano Lett.*, **2009**, *9*, 220–224.

(12) Rao, S. S.; Jammalamadaka, S. N.; Stesmans, A.; Moshchalkov, V. V.; Tol, J. V.; Kosynkin, D. V.; Higginbotham-Duque, A.; Tour, J. M. Ferromagnetism in Graphene Nanoribbons: Split versus Oxidative Unzipped Ribbons. *Nano letters*, **2012**, *12*, 1210-1217.

(13) Sepioni, M.; Nair, R. R.; Rablen, S.; Narayanan, J.; Tuna, F.; Winpenny, R.; Geim, A. K.; Grigorieva, I. V. Limits on Intrinsic Magnetism in Graphene. *Phys Rev Lett*, **2010**, *105*, 207205:1-4.

(14) Li, L.; Qin, R.; Li, H.; Yu, L.; Liu, Q.; Luo, G.; Gao, Z.; Lu, J. Functionalized Graphene for High-Performance Two-Dimensional Spintronics Device. *ACS Nano*, **2011**, *5*, 2601–2610.

(15) Lee, S. U.; Belosludov, R. V.; Mizuseki, H.; Kawazoe, Y. Designing Nanogadgetry for Nanoelectronic Devices with Nitrogen-Doped Capped Carbon Nanotubes. *Small*, **2009**, *5*, 1769–1775.

(16) Li, Y. F.; Zhou, Z.; Shen, P. W.; Chen, Z. F. Spin Gapless Semiconductor−Metal−Half-Metal Properties in Nitrogen-Doped Zigzag Graphene Nanoribbons. *ACS Nano*, **2009**, *3*, 1952–1958.

(17) . Ma, Y. C.; Foster, A. S.; Krasheninnikov, A.V.; Nieminen, R. M. Nitrogen in graphite and carbon nanotubes: Magnetism and mobility. *Phys. Rev. B*, **2005**, *72*, 205416:1-6

(18) Ma, C. C.; Shao, X. H.; Cao, D. P. Nitrogen-doped graphene nanosheets as anode materials for lithium ion batteries: a first-principles study. *J. Mater. Chem.*, **2012**, *22*, 8911–8915.

(19) Zhang, Y.; Talapatra, S.; Kar, S.; Vajtai, R.; Nayak, S. K.; Ajayan, P. M. First-Principles Study of Defect-Induced Magnetism in Carbon. *Phys. Rev. Lett*., **2007**, *99*, 107201:1-4.

(20) Dai, J. Y.; Yuan, J. M. Adsorption of molecular oxygen on doped graphene: Atomic, electronic, and magnetic properties. *Phys. Rev. B*, **2010**, *81*, 165414:1-7.

(21) Liu, Y.; Tang, N.; Wan, X.; Feng, Q.; Li, M.; Xu, Q.; Liu, F.; Du, Y. Realization of ferromagnetic graphene oxide with high magnetization by doping graphene oxide with nitrogen. *Sci. Rep.*, **2013**, *3*, 2566:1-5.

(22) Jalili, S.; Vaziri, R. Study of the electronic properties of Li-intercalated nitrogen doped graphite. *Mol. Phys*., **2011**, *109*, 687-694.

(23) . Ferrari, A. C. ; Meyer, J. C.; Scardaci, V.; Casiraghi, C.; Lazzeri, M.; Mauri, F.; Piscanec, S.; Jiang, D.; Novoselov, K. S.; Roth. S.; Geim, A. K. Raman Spectrum of Graphene and Graphene Layers. *Phys. Rev. Lett*., **2006**, *97*, 187401:1-4.

(24) Ferrari, A. C. Raman spectroscopy of graphene and graphite: Disorder, electron–phonon coupling, doping and nonadiabatic effects. *Solid State Commun*., **2007**, *143*, 47–57.

(25) Tuinstra, F.; Koenig, J. L. Raman Spectrum of Graphite. *J. Chem. Phys*., **1970**, *53*, 1126-1130.

(26) Ferrari, A. C.; Robertson, Interpretation of Raman spectra of disordered and amorphous carbon. *J. Phys. Rev. B*, **2000**, *61*, 14095-14107.

(27) Wu, W.; Yu, Q.; Peng, P.; Liu, Z.; Bao, J.; Pei, S. S. Control of thickness uniformity and grain size in graphene films for transparent conductive electrodes. *Nanotechnology*, **2012**, *23*, 035603:1-8.

(28) Soin, N.; Roy, S. S.; Roy, S.; Hazra, K. S.; Misra, D. S.; Lim, T. H.; Hetherington, C. J. D; McLaughlin, J. A. Enhanced and Stable Field Emission from in Situ Nitrogen-Doped Few-Layered Graphene Nanoflakes. *J. Phys. Chem. C*, **2011**, *115*, 5366–5372.

(29) Subrahmanyam, K. S.; Panchakarla, L. S.; Govindaraj, A.; Rao, C. N. R. Simple Method of Preparing Graphene Flakes by an Arc-Discharge Method. *J. Phys. Chem. C*, **2009**, *113*, 4257–4259.

(30) Pisana, S.; Lazzeri, M.; Casiraghi, C.; Novoselov, K. S.; Geim, A. K.; Ferrari, A. C.; Mauri, F. Breakdown of the adiabatic Born-Oppenheimer approximation in graphene. *Nat. Mater*., **2007**, *6*, 198–201.

(31) Yan, J.; Zhang, Y.; Kim, P.; Pinczuk, A. Electric field effect tuning of electron-phonon coupling in graphene. *Phys. Rev. Lett*., **2007**, *98*, 166802:1-4.

(32) Eckmann, A.; Felten, A.; Mishchenko, A.; Britnell, L.; Krupke, R.; Novoselov, K.S.; Casiraghi, C. Probing the nature of defects in graphene by Raman spectroscopy. *Nano Lett*., **2012,** *12*, 3925-3930.

(33) Ray, S.C.; Soin, N.; Magkato, T.; Chuang, C.H.; Pong, W.F.; Roy, S.S.; Ghosh, S.K.; Strydom, A.M.; McLaughlin, J.A.; Graphene supported graphone/graphane bilayer nanostructure material for spintronics. *Sci. Rep.*, **2014**, *4*, 3862:1-7.

(34) Abbas, G.; Papakonstantinou, P.; Iyer, G.R.; Kirkman, I.W.; Chen, L.C; Substitutional nitrogen incorporation through rf glow discharge treatment and subsequent oxygen uptake on vertically aligned carbon nanotubes. *Phys. Rev. B,* **2007**, *75*, 195429:1-9.

(35) Pao, C.W.; Ray, S.C.; Tsai, H.M.; Chen, Y.S.; Chen, H.C.; Lin, I.N.; Pong, W.F.; Chiou, J.W.; Shang,N.G.; Papakonstantinou, P. Change of Structural Behaviors of Organo-silane Exposed Graphene Nanoflakes. *J. Phys. Chem. C*, **2010**, *114*, 8161–8166.

(36) Fagan, S.B.; Mota, R.; Baierle, R.J.; DaSilva, A.J.R.; Fazzio, A. Ab initio study of an organic molecule interacting with a silicon-doped carbon nanotube. *Dia. Relat. Mater.*, **2003**, *12*, 861–863.

(37) Chiou, J.W.; Ray, S.C.; Peng, S.I.; Chuang, C.H.; Wang, B.Y.; Tsai, H.M.; Pao, C.W.; Lin, H.J.; Shao,Y.C.; Wang,Y.F.; Chen, S.C. Nitrogen-Functionalized Graphene Nanoflakes (GNFs:N): Tunable Photoluminescence and Electronic Structures. *J. Phys. Chem. C*, **2012**, *116*, 16251–16258.

(38) Ray, S.C.; Palnitkar, U.; Pao, C.W.; Tsai, H.M.; Pong, W.F.; Lin, I.N.; Papakonstantinou, P.; Ganguly, A.; Chen, L.C.; Chen, K.H. Field emission effects of nitrogenated carbon nanotubes on chlorination and oxidation. *J. Appl. Phys.*, **2008**, *104*, 063710.

(39) Ray, S.C.; Mbiombi, W.; Papakonstantinou, P. Electrical and electronic properties of nitrogen doped amorphous carbon (a-CNx) thin films. Curr. *Appl. Phys.*, **2014,** *14*, 1845–1848.

(40) Ray, S.C.; Chiou, J.W.; Pong, W.F.; Tsai,M.H. The electronic properties of nanomaterials elucidated by synchrotron radiation-based spectroscopy. *Crit. Rev. Solid State Mater. Sci*., **2006**, *31*, 91–110.

(41) Ray, S.C.; Bao, C.W.; Tsai, H.M.; Chiou, J.W.; Jan, J.C.; Kumar, K.K.; Pong, W.F.; Tsai, M.H.; Wang, W.J.; Hsu, C.J.; Okpalugo, T. I. T. Electronic structure and bonding properties of SiSi-doped hydrogenated amorphous carbon films. *Appl. Phys. Lett.*, **2004**, *85*, 4022–4024.

(42) Terekhov, V. A. ; Terukov, E. I.; Trapeznikova, I. N.; Kashkarov, M.; Kurilo, O. V.; Turishchev, S. Y.; Golodenko, A. B.; Domashevskaya, E. P. A study of the local electronic and atomic structure in a-SixC1−x amorphous alloys using ultrasoft X-ray emission spectroscopy. *Semiconductors*, **2005**, *39*, 830–834.

(43) Pacilé, D.; Papagno, M.; Rodríguez, A.F.; Grioni, M.; Papagno, L.; Girit, Ç.Ö.; Meyer, J. C. ; Begtrup, G. E.; Zettl, A.; Near-Edge X-Ray Absorption Fine-Structure Investigation of Graphene. *Phys. Rev. Lett*. **2008**, *101*, 066806:1-4.

(44) Usachov, D.; Vilkov, O.; Gruneis, A.; Haberer, D.; Fedorov, A.; Adamchuk, V.K.; Preobrajenski, A.B.; Dudin, P.; Barinov, A.; Oehzelt, M.; Laubschat, C. Nitrogen-doped graphene: efficient growth, structure, and electronic properties. *Nano lett.*, **2011**, *11*, 5401-5407.

(45) Li, X.; Hua, W.; Guo, J.; Luo, Y. Electronic Structure of Nitrogen-Doped Graphene in the Ground and Core-Excited States from First-Principles Simulations. *J. Phys. Chem. C*, **2015**, *119*, 16660-16666.

(46) Geng, D.; Yang, S.; Zhang, Y.; Yang, J.; Liu, J.; Li, R.; Sham,T.K.; Sun, X.; Ye, S.; Knights, S. Nitrogen doping effects on the structure of graphene. *Appl. Surf. Sci*., **2011**, *257*, 9193–9198.

(47) Dai, G. P.; Zhang, J. M.; Deng, S. Synthesis and characterization of nitrogen-doped monolayer and multilayer graphene on TEM copper grids. *Chem. Phys. Lett.*, **2011**, *516*, 212-215.

(48) Ray, S. C. ; Pao, C. W.; Chiou, J. W.; Tsai, H. M.; Jan, J. C.; Pong, W. F.; McCann, R.; Roy, S. S.; Papakonstantinou, P.; McLaughlin, J. A. Electronic properties of a-CNx thin films: An x-ray-absorptiona nd photoemission spectroscopy study. *J. Appl. Phys.*, **2005**, *98*, 033708:1-4.

(49) Gago, R.; Jiménez, I.; Neidhardt, J.; Abendroth, B.; Caretti, I.; Hultman, L.; MÖller, W. Correlation between bonding structure and microstructure in fullerenelike carbon nitride thin films. *Phys. Rev. B*, **2005**, *71*, 125414-6.

(50) Li, J.; Li, X.; Zhao, P.; Lei, D. Y.; Li, W.; Bai, J.; Ren Z.; Xu, X. Searching for magnetism in pyrrolic N-doped graphene synthesized via hydrothermal reaction. *Carbon*, **2015**, *84*, 460-468.

(51) Zhao, W.; Hofert, O.; Gotterbarm, K.; Zhu, J.F.; Papp, C.; Steinrück, H.-P. Production of nitrogen-doped graphene by low-energy nitrogen implantation. J. Phys. Chem. C, 2012, 116, 5062-5066.

(52) Sakulsermsuk, S.; Singjai P.; Chaiwong, C. Influence of plasma process on the nitrogen configuration in graphene. *Diamond Relat. Mater.*, **2016**, *70*, 211-218.

(53) Iyer, G. R.; Maguire, P.D.; Metal free, end-opened, selective nitrogen-doped vertically aligned carbon nanotubes by a single step in situ low energy plasma process. *J. Mater. Chem.*, **2011**, *21*, 16162-16169.

(54) Åhlgren, E. H.; Kotakoski, J.; Krasheninnikov, A. V. Atomistic simulations of the implantation of low energy boron and nitrogen ions into graphene. *Phys. Rev. B*, **2011,** *83(11)*, 115424:1-7

(55) Bhattacharyya, S.; Cardinaud, C.; Turban, G. Spectroscopic determination of the structure of amorphous nitrogenated carbon films. *J. Appl. Phys.*, **1998**, *83*, 4491-4500.

(56) Shao, Y.; Zhang, S.; Engelhard, M.H.; Li, G.; Shao, G.; Wang, Y.; Liu, J.; Aksay, I.A.; Lin,Y. Nitrogen - doped graphene and its electrochemical applications. *J. Mater. Chem.*, **2010**, *20*, 7491-7496.

(57) Li, X.; Wang, H.; Robinson, J. T.; Sanchez, H.; Diankov, G.; Dai, H. Simultaneous nitrogen doping and reduction of graphene oxide. *J. Am. Chem. Soc.*, **2009,** *131*, 15939-15944.

(58) Souto, S.; Pickholz, M.; Santos, M.C. Dos; Alvarez, F. Electronic structure of nitrogen-carbon alloys (a-CNx) determined by photoelectron spectroscopy. *Phy. Rev. B*, **1998**, *57*, 2536-2540.

(59) Bianconi, A.; Hagström, S. B. M.; Bachrach, R. Z. Photoemission studies of graphite high-energy conduction-band and valence-band states using soft-x-ray synchrotron radiation excitation. *Phys. Rev. B*, **1977**, *16*, 5543-5548.

(60) Becerril, H. A.; Mao, J.; Liu, Z.; Stoltenberg, R. M.; Bao, Z.; Chen, Y. Evaluation of solution-processed reduced graphene oxide films as transparent conductors. *ACS Nano*, **2008**, *2*, 463-470.

(61) Larciprete, R.; Gardonio, S.; Petaccia, L.; Lizzit, S. Atomic oxygen functionalization of double walled C nanotubes. *Carbon*, **2009**, *47*, 2579-2589.

(62) Luo, Z.; Lim, S.; Tian, Z.; Shang, J.; Lai, L.; MacDonald, B.; Fu, C.; Shen, Z.; Yu, T.; Lin. J. Pyridinic N doped graphene: synthesis, electronic structure, and electrocatalytic property. *J. Mater. Chem.*, **2011**, *21*, 8038-8044.

(63) Miao, Q.; Wang, L. ; Liu, Z.; Wei, B.; Xu, F.; Fei, W. Magnetic properties of N-doped graphene with high Curie temperature. *Sci. Rep.*, **2016**, *6*, 21832:1-10.

(64) Ito, Y. ; Christodoulou, C.; Nardi, M. V. ; Koch, N. ; Kläui, M. ; Sachdev, H.; Müllen, K. ; Tuning the Magnetic Properties of Carbon by Nitrogen Doping of Its Graphene Domains. *J. Am. Chem. Soc.*, **2015**, *137*, 7678-7685.

(65) He, Z.; Yang, X.; Xia, H.; Zhou, X.; Zhao, M.; Song, Y.; Wang, T. Enhancing the ferromagnetization of graphite by successive 12 C+ ion implantation steps. *Carbon*, **2011**, *49*, 1931–1938.

(66) Jalili, S.; Vaziri, R.; Study of the Electronic Properties of Li-Intercalated Nitrogen doped Graphite Molecular Physics. *Mol. Phys.*, **2011**, *109*, 687–694.

(67) Talapatra, S.; Ganesan, P. G.; Kim, T.; Vajtai, R.; Huang, M.; Shima, M.; Ramanath, G.; Srivastava, D.; Deevi, S. C.; Ajayan, P. M. Irradiation-Induced Magnetism in Carbon Nanostructures. *Phys. Rev. Lett.*, **2005**, *95*, 097201:1-4.

(68) Błoński, P.; Tuček, J.; Sofer, Z.; Mazánek, V.; Petr, M.; Pumera, M.; Otyepka M.; Zbořil, R. Doping with Graphitic Nitrogen Triggers Ferromagnetism in Graphene. *J. Am. Chem. Soc.* ***2017***, *139*, 3171-3180.

• FIGURE CAPTIONS

Figure 1 (a) Deconvoluted Raman spectra of pristine and functionalised FLG samples showing the variation of the peak positions of the D and G bands, (b) electron field emission behaviour showing current density (J) as a function of applied electric field (E_A) with the inset showing the Fowler–Nordheim plot obtained from EFE measurements.

Figure 2: (a) C *K*-edge XANES spectra of the pristine and nitrogenated FLGs with the lower inset showing the signatures of C–H bonds and interlayer graphite states. The inset above shows the changes in the C 1s core level XPS spectra, (b) N K-edge XANES spectra of the ECR and rf-PECVD functionalised with their respective deconvolutions in (c) and (d) respectively.

Figure 3: C1s, O1s core level XPS spectra of (a, d) pristine FLG, (b, e) rf-PECVD nitrogenated FLG, (c, f) ECR nitrogenated FLG. (g) deconvoluted N1s core level spectra of ECR nitrogenated FLG with the corresponding spectra for rf-PECVD sample shown in (h).

Figure 4: (a) UPS He-I and (b) He-II spectra for the measurement of work function and density of states below the Fermi level, respectively. The change of the chemical composition and arising bonding modification as observed in the distinct hybridised bands observed for deconvoluted spectra for (c) FLG, (d) rf-PECVD nitrogenated FLG and (e) ECR functionalised FLG, respectively.

Figure 5: Magnetic hysteresis loops obtained for (a) FLG, (b) rf-PECVD nitrogenated FLG and (c) ECR nitrogenated FLG at 40K and 300K, respectively. AFM scans for pristine FLG and ECR nitrogenated FLG with the corresponding MFM scans shown in (j-l) and (m-o), respectively. The significant increase and localisation of the magnetic domains in the ECR N-graphene is clearly visible in the amplitude scans.

Table 1: Elemental Quantification, magnetic parameters and Raman parameters

Samples	Element and quantification (at%)			Electron field emission		Magnetic parameters				Raman Parameters	
	C	O	N	E_0 (V/μm) (TOE)	J (mA/cm^2) @ 32 V/μm	Temperature (K)	Hc (Coercivity) (Oe)	Ms (Saturation magnetisation) (emu/gm)	Mr (Remnant magnetisation) (emu/gm)	(I_D/I_G)	(I_{2D}/I_G)
FLG	78.78	21.22	--	26.5	0.18	40 300	112.37 62.98	3.47×10^{-4} 2.60×10^{-4}	0.52×10^{-4} 0.42×10^{-4}	0.62	1.04
FLG:N (PECVD)	78.41	18.53	4.06	40.0	1.16	40 300	80.30 80.41	0.39×10^{-4} 0.42×10^{-4}	0.09×10^{-4} 0.12×10^{-4}	0.70	0.70
FLG:N (ECR)	78.05	19.77	2.18	20	2.97	40 300	40.00 25.42	118.62×10^{-4} 111.91×10^{-4}	9.74×10^{-4} 6.04×10^{-4}	1.02	0.79

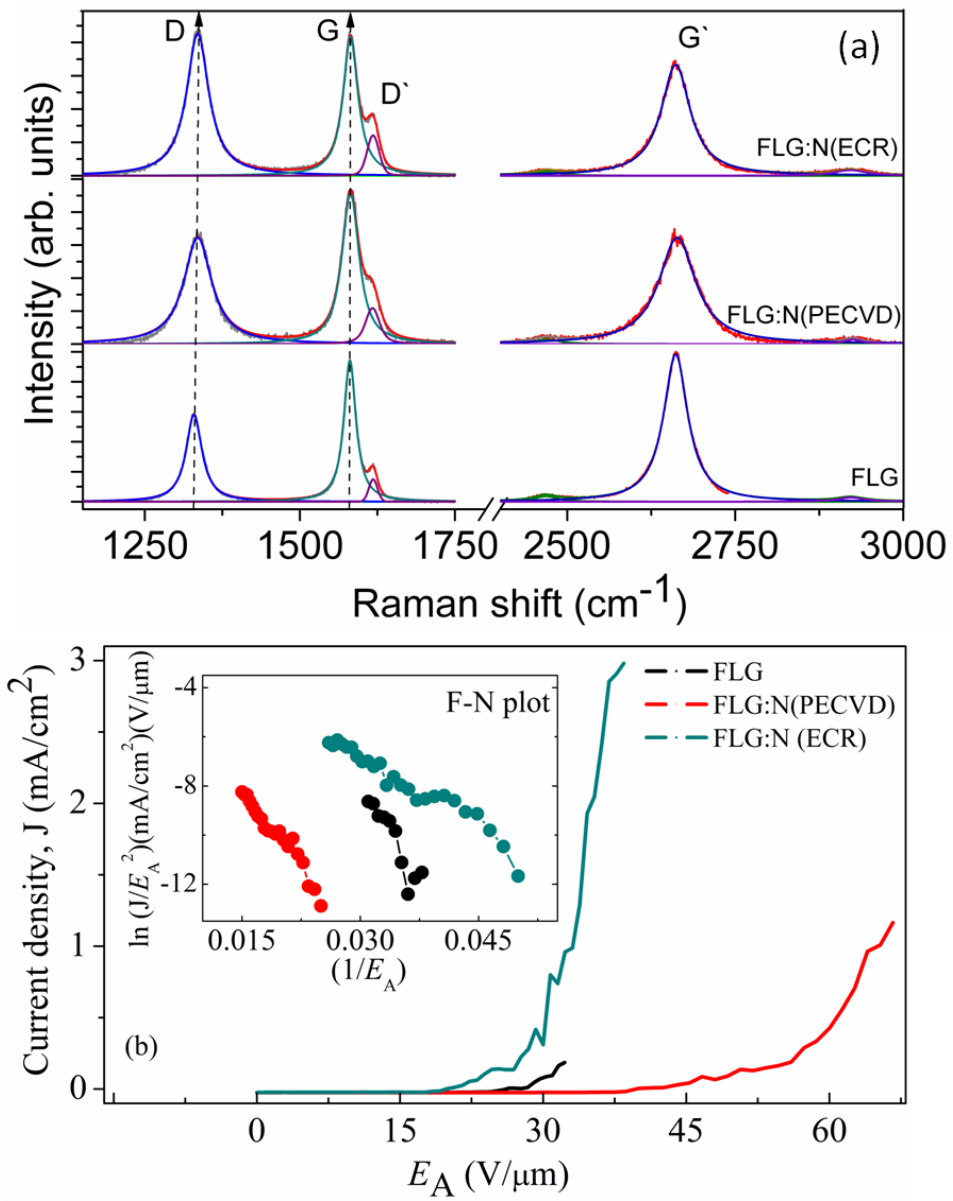
D
G
D`
G`
(a)
FLG:N(ECR)
FLG:N(PECVD)
FLG
Intensity (arb. units)
1250
1500
1750
2500
2750
3000
Raman shift (cm-1)
F-N plot
ln (J/EA2)(mA/cm2)(V/μm)
(1/EA)
(b)
FLG
FLG:N(PECVD)
FLG:N (ECR)
Current density, J (mA/cm2)
EA (V/μm)

Figure 1

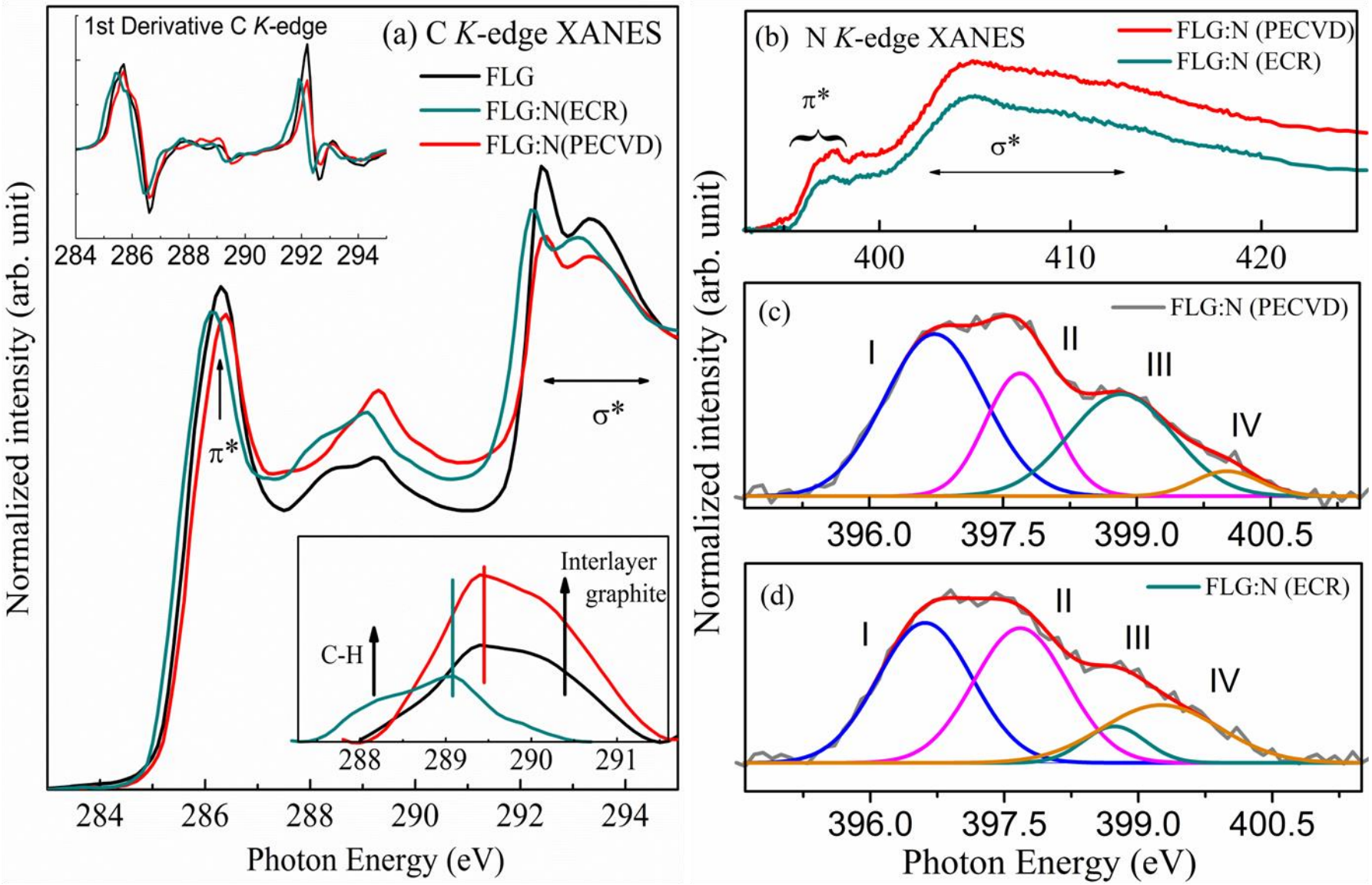
(a) C K-edge XANES
1st Derivative C K-edge
FLG
FLG:N(ECR)
FLG:N(PECVD)
π*
σ*
C-H
Interlayer graphite
Normalized intensity (arb. unit)
Photon Energy (eV)
(b) N K-edge XANES
FLG:N (PECVD)
FLG:N (ECR)
(c)
(d)
I
II
III
IV

Figure 2

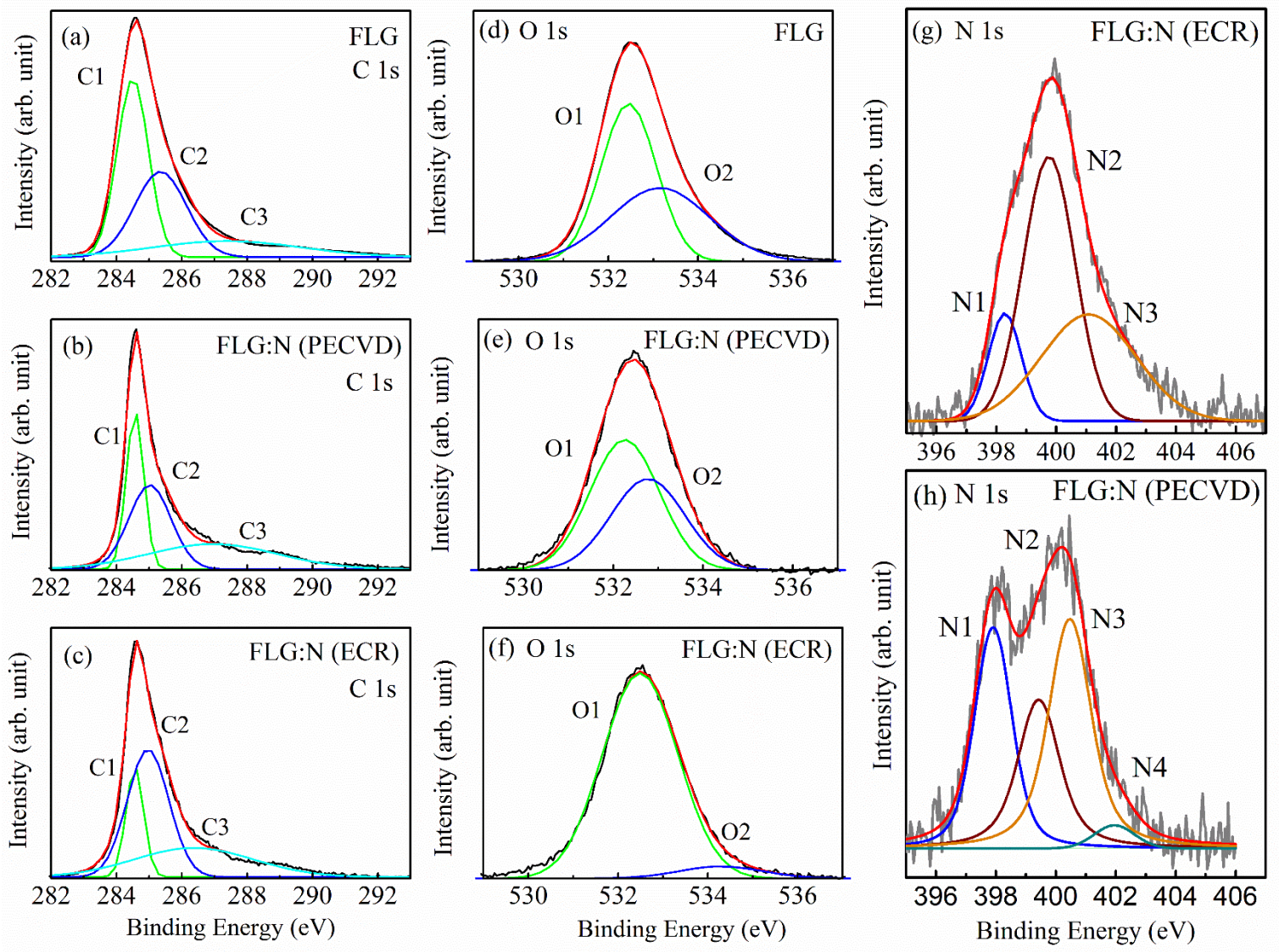
(a) C 1s FLG
C1
C2
C3
(b) C 1s FLG:N (PECVD)
C1
C2
C3
(c) C 1s FLG:N (ECR)
C1
C2
C3
Intensity (arb. unit)
282 284 286 288 290 292
Binding Energy (eV)
(d) O 1s FLG
O1
O2
(e) O 1s FLG:N (PECVD)
O1
O2
(f) O 1s FLG:N (ECR)
O1
O2
530 532 534 536
Binding Energy (eV)
(g) N 1s FLG:N (ECR)
N1
N2
N3
(h) N 1s FLG:N (PECVD)
N1
N2
N3
N4
396 398 400 402 404 406
Binding Energy (eV)

Figure 3

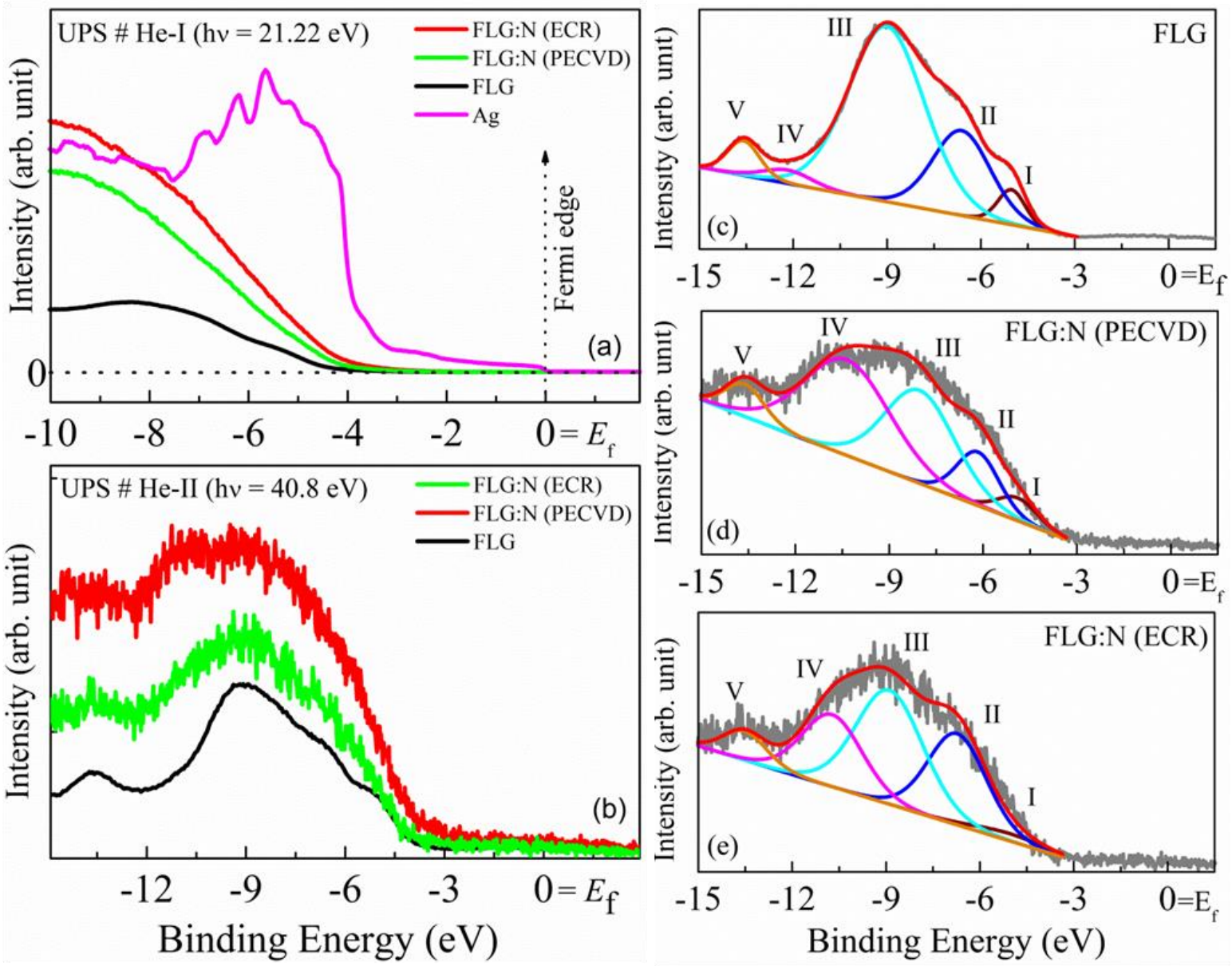
UPS # He-I (hν = 21.22 eV)
FLG:N (ECR)
FLG:N (PECVD)
FLG
Ag
Fermi edge
Intensity (arb. unit)
(a)
0
-10
-8
-6
-4
-2
0 = E_f
UPS # He-II (hν = 40.8 eV)
FLG:N (ECR)
FLG:N (PECVD)
FLG
Intensity (arb. unit)
(b)
-12
-9
-6
-3
0 = E_f
Binding Energy (eV)
FLG
III
V
IV
II
I
(c)
Intensity (arb. unit)
-15
-12
-9
-6
-3
0=E_f
FLG:N (PECVD)
IV
V
III
II
I
(d)
Intensity (arb. unit)
-15
-12
-9
-6
-3
0=E_f
FLG:N (ECR)
III
IV
V
II
I
(e)
Intensity (arb. unit)
-15
-12
-9
-6
-3
0=E_f
Binding Energy (eV)

Figure 4

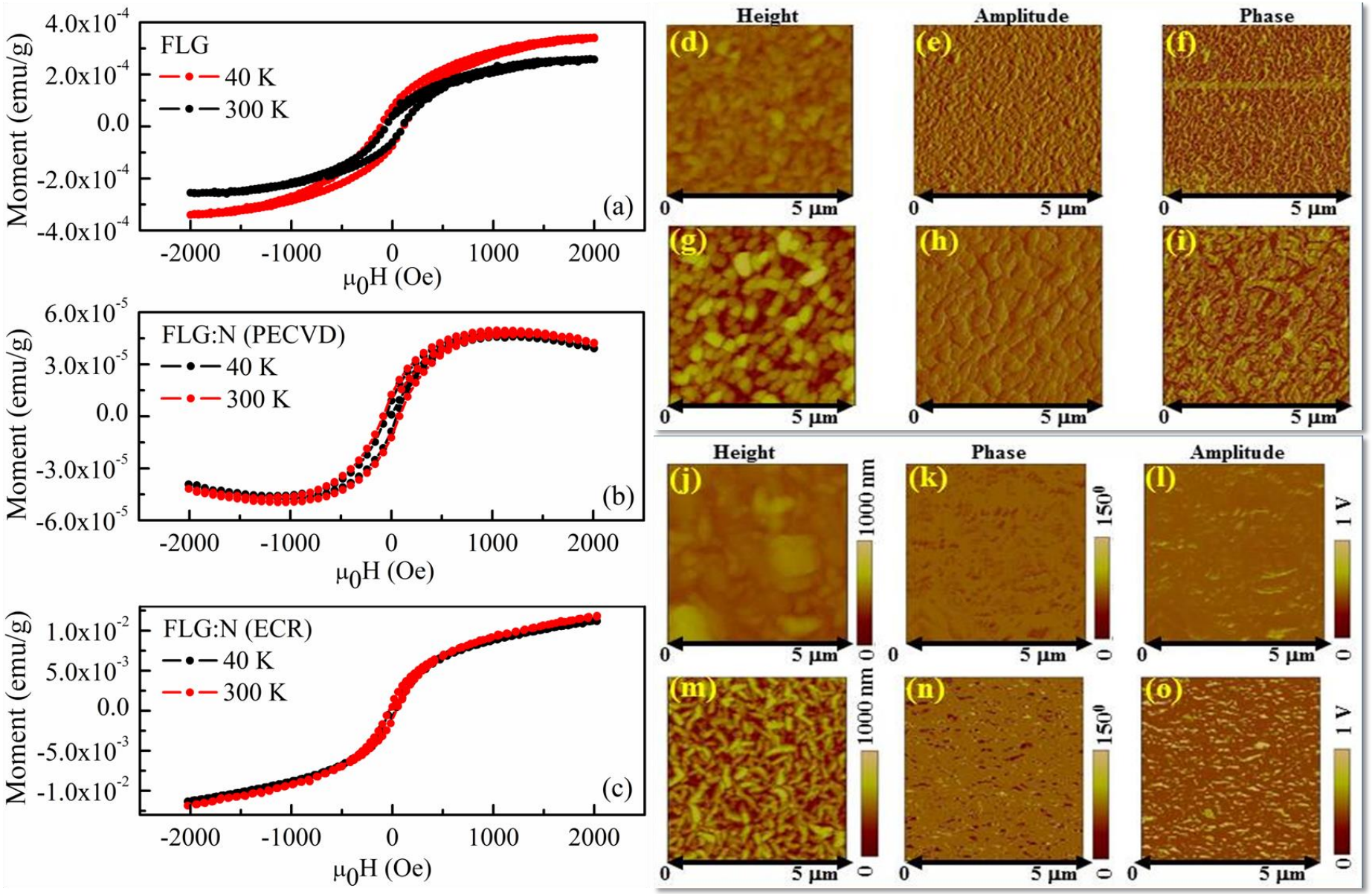
FLG
40 K
300 K
Moment (emu/g)
μ_0H (Oe)
(a)
FLG:N (PECVD)
40 K
300 K
(b)
FLG:N (ECR)
40 K
300 K
(c)
Height
Amplitude
Phase
(d)
(e)
(f)
(g)
(h)
(i)
(j)
(k)
(l)
(m)
(n)
(o)
5 µm
1000 nm
150⁰
1 V

Figure 5